From nanoscale to microscale: crossover in the diffusion dynamics within two pyrrolidinium-based ionic liquids

Mose' Casalegno*[a], Guido Raos[a], Giovanni Battista Appetecchi[b], Stefano Passerini[c,d], Franca Castiglione*[a] and Andrea Mele[a]

a Department of Chemistry, Materials and Chemical Engineering "G. Natta", Politecnico di Milano, Piazza L. Da Vinci, 32, 20133 Milano, Italy

b ENEA, Italian National Agency for New Technology, Energy and Sustainable Economic Development, Materials and Physicochemical Processes Laboratory, Via Anguillarese 301, Rome, Italy

c Helmholtz Institute Ulm, Karlsruhe Institute of Technology, Helmholtzstrasse 11, Ulm, Germany

d Karlsruhe Institute of Technology, P.O. Box 3640, Karlsruhe, Germany

ABSTRACT

Knowledge of the ion motion in room temperature ionic liquids (RTILs) is critical for their applications in a number of fields, from lithium batteries to dye-sensitized solar cells. Experiments on a limited number of RTILs have shown that, on macroscopic time-scales, the ions typically undergo conventional, Gaussian diffusion. On shorter time-scales, however, non-Gaussian behavior has been observed, similar to supercooled fluids, concentrated colloidal suspensions, and more complex systems. Here we characterize the diffusive motion of ionic liquids based on the N-butyl-N-methylpyrrolidinium (PYR_{14}) cation and bis(trifluoro methanesulfonyl)imide (TFSI) or bis(fluorosulfonyl)imide (FSI) anions. A combination of pulsed gradient spin-echo (PGSE) NMR experiments and Molecular Dynamics (MD) simulations demonstrates a cross-over from subdiffusive behavior to conventional Gaussian diffusion at about 10 ns. The deconvolution of molecular displacements into a continuous spectrum of diffusivities shows that the short-time behavior is related to the effects of molecular caging. For PYR_{14}FSI, we identify the change of short-range ion-counterion associations as one possible mechanism triggering long-range displacements.

TOC GRAPHICS

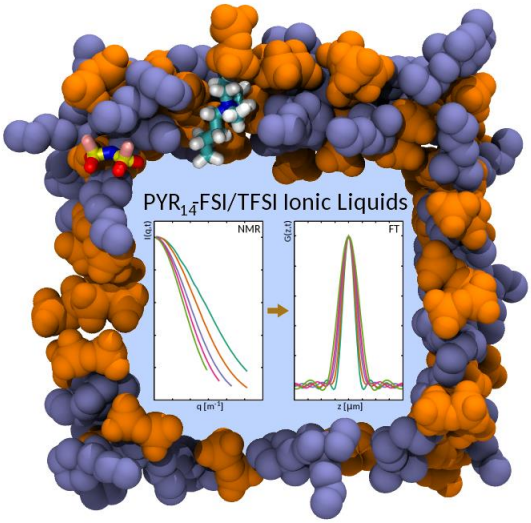

KEYWORDS Ionic liquids, PGSE NMR, Diffusion, Pyrrolidinium cation, Molecular dynamics

Room temperature ionic liquids (RTILs) represent an important and broad class of salts characterized by melting temperatures around room temperature. The low vapor pressure, high electrochemical and thermal stability, and high ionic conductivity make them well suited for several applications, including lithium batteries, sensors, dye-sensitized solar cells, fuel cells, capacitors, hydrogen storage and catalysis.[1–6] In principle, by a careful selection of the cations and anions, their chemical-physical properties can be tailored to the application of interest. In practice, however, the synthesis and characterization of a large number of potentially interesting candidates is both time- and resource-consuming. In this perspective, a better understanding of the relationship between molecular structure and physicochemical properties can be extremely valuable, and may help to fully exploit the potential of these materials.

The transport properties of RTILs are especially relevant, in view of their application as electrolytes. During the past decade, significant efforts have been put in understanding the complex dynamics of these systems. Studies based on NMR experiments[7,8] have evidenced that, on a macroscopic time-scale, ion diffusion in the bulk liquid phase is essentially unrestricted and Gaussian, albeit with generally small diffusion coefficients. On shorter timescales, early indications of non-Gaussian diffusion in RTILs were provided by MD studies[9-14] and associated to dynamical heterogeneities, e.g., transient spatial fluctuations in the local dynamical behavior.[15] According to this view, the mobility of the individual ions in the bulk may vary over a wide range, due to local fluctuations in the fluid structure, similar to those observed in supercooled fluids,[16–19] concentrated colloidal suspensions[20,21] and more complex systems.[22,23] At the molecular level, dynamical heterogeneity is usually associated with caging phenomena. The molecules inhabit transient cages formed by their nearest neighbours. Most of the time, the molecules "rattle" around well-defined positions within the cage. Occasional cage

rearrangements, however, may promote large displacements, allowing the molecule to "jump" from one cage to another. In turn, the displacement of one molecule triggers the rearrangement of the its nearest neighbors, so that these correlated motions result in the transient formation of higher mobility pockets within a lower mobility matrix. The strong Coulomb interactions among the ions, in combination with other effects such as Van der Waals and hydrogen bonding interactions and the conformational flexibility of the ions, further enhance the importance of these correlation effects.

Although this picture may qualitatively explain non-Gaussian diffusion in RTILs, its details are often difficult to capture and require a close integration of experiments, computation and theory.[24–28] The complex organization of these liquids is susceptible to change significantly upon changing the ion structure and, even for the same system, the interpretation of the experimental or numerical data may not be univocal. For example, non-gaussianity in Emim-NO_3 was attributed to the effect of long-range Coulombic interactions,[9] whereas in Bmim-BF_4 to the formation of polar and non-polar domains.[29] In another study on Bmim-PF_6,[30] the differences in ion mobilities were linked to the existence of locally heterogeneous environments, and ultimately related to ionic nearest-neighbor interactions. In parallel with computational studies, quasi-elastic neutron scattering (QENS) experiments[31–33] have evidenced the existence of distinct relaxation mechanisms for some RTILs, with a slower one (α) related to spatially restricted translational diffusion and a faster one (β) to conformational motion of molecular sub-structures, like alkyl side-chains.[32,33]

In this manuscript we analyze the translational dynamics of two RTILs based on N-butyl-N-methylpyrrolidinium (PYR_{14}) as cation and bis(trifluoromethanesulfonyl)imide (TFSI) or bis(fluorosulfonyl)imide (FSI) as anions. Our interest in these systems is motivated by their

importance in the field of lithium-ion batteries.[34–38] Furthermore, while imidazolium-based systems have been quite extensively characterized,[11,14,31] less information is available for pyrrolidinium-based RTILs. Experimentally, the dynamical behavior of these systems has been investigated by means of pulsed gradient spin-echo (PGSE) NMR spectroscopy. In addition to this technique, which was already been used by us[39,40] and other[41–43] groups, we employ also MD simulations. In doing so, our aim is to cross-validate the experimental and numerical results, as well as to obtain structural information and provide a consistent description of the ion dynamics, from the sub-ns to the ms time scale.

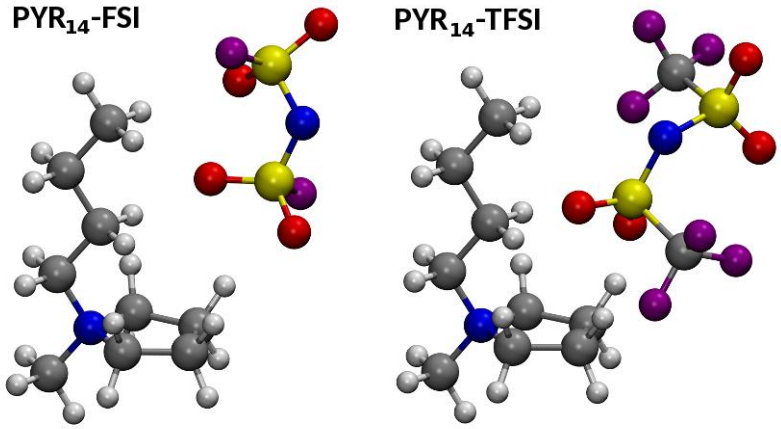

Scheme 1. Sketches of the molecular structures investigated in this work.

PGSE-NMR spectroscopy is able to encode the molecular spatial position by employing pulsed magnetic field gradients of varying intensity. At t=0, certain nuclei within the probe molecules are labeled by the pulsed field gradient according to their position. After diffusion has occurred over a certain time t, the observed signal intensity $I(q,t)$ is attenuated depending on the net molecular mean-square displacement (MSD) and on an experimental parameter $q=2\pi g\gamma\delta$. This combines the magnetogiric ratio of the observed nuclei (γ), the applied field gradient (g)

and gradient pulse duration (δ) (see the Supporting Information for experimental details). Note that q has the dimension of a reciprocal distance. The value of t determines the time-scale of the dynamical information that can be extracted from the NMR experiment. In an isotropic system, the MSD along the pulsed field gradient axis (z) is statistically equivalent to that along the orthogonal directions (x and y), and therefore we have:

$$\left\langle z^2(t)\right\rangle = \frac{1}{3}\left\langle \left(\mathbf{r}(t)-\mathbf{r}(0)\right)^2\right\rangle \tag{1}$$

where $\mathbf{r}(t)$ is the position of the tagged species at time t, $\mathbf{r}(0)$ is its starting position and $\langle\bullet\rangle$ indicates an average over all nuclei.

The mathematical treatment of PGSE-NMR data can follow two complementary approaches:

1) *The gradient-dependent echo decay (GDED) analysis.* The echo decay $I(q,t)$ is related as follows to the MSD of the nuclei along the pulsed field gradient axis:

$$I(q,t) = I(0,t)\exp\left(-\frac{1}{2}q^2\left\langle z^2(t)\right\rangle\right). \tag{2}$$

The MSD of the diffusing nuclei increases with the observation time t. The following general relationship holds for an isotropic system:

$$\left\langle z^2(t)\right\rangle = 2Dt^{\alpha} \tag{3}$$

Unrestricted, Fickian diffusion—here we follow refs. 22 and 23 in using this term—occurs when $\alpha=1$ and the proportionality constant D is then a true diffusion coefficient. In addition, it is possible to observe also subdiffusive ($0<\alpha<1$) and superdiffusive ($\alpha>1$) motion. The same system may exhibit all of these translational regimes, depending on the observation time window. We also point out that conventional Fickian diffusion ($\alpha=1$) does not necessarily correspond to a Gaussian distribution of displacement probabilities.[22,23] For this reason, it makes sense to refine data analysis by the *q-space* approach described below.

2) *The q-space analysis.* This is an alternative approach used to analyze PGSE experiments.[44] The *q-space* theory, developed for heterogeneous systems and biological tissues[45,46], describes the NMR diffusion measurements in terms of displacement probabilities. In analogy with scattering methods, the reciprocal vector q can be considered as a probe of the reciprocal space of spin displacements. According to this theory, the echo attenuation is the Fourier transform (FT) of the displacement probabilities G_{NMR} along the z axis. Thus G_{NMR} can be recovered by the inverse FT:

$$G_{NMR}(z,t) = \int_{-\infty}^{+\infty} I(q,t) e^{iqz} dq \tag{4}$$

This is actually the Van Hove self-correlation function, which will be formally defined below in connection with the MD simulations. In the case of conventional diffusion, combining Eq. (2) and Eq.(3) (with α=1), G_{NMR} is a Gaussian function:

$$G_{NMR}(z,t) = I_0 \sqrt{\frac{\pi}{Dt}} \exp^{-\frac{z^2}{4Dt}} . \tag{5}$$

In this case, increasing t widens the profile as the molecules can travel longer distances, and the diffusion coefficient D can be calculated from the full width at half-maximum:

$$\Delta(z_{0.5}) = 2[4Dt \ln 2]^{1/2} . \tag{6}$$

Instead, for a restricted motion (e.g., in heterogeneous or porous materials), no difference should be observed once $\langle z^2(t) \rangle^{1/2}$ becomes comparable with the length scale of the heterogeneities which provide the restriction.

	NMR		MD	
	$PYR_{14}FSI$	$PYR_{14}TFSI$	$PYR_{14}FSI$	$PYR_{14}TFSI$
D_H (m^2/s)	3.28×10^{-11}	2.48×10^{-11}	3.42×10^{-11}	2.25×10^{-11}
D_F (m^2/s)	4.02×10^{-11}	2.04×10^{-11}	3.63×10^{-11}	2.04×10^{-11}

Table 1. PGSE-NMR and MD diffusion coefficients of the cations (D_H) and the anions (D_F) within the two RTILs.

For all species, we have initially analyzed our experimental data following GDED approach, Figure 1 shows the log-log plots of the MSDs obtained from the measurements performed on the cation (^1H) and anion (^{19}F) of both RTILs, for diffusion times t in the range 0.2-0.7 s. We found $\langle z^2 \rangle$ to vary linearly with time, thereby indicating Fickian diffusion over this time scale in both $PYR_{14}FSI$ and $PYR_{14}TFSI$. The results have been collected in Table 1. Both D_H and D_F are higher for $PYR_{14}FSI$ than for $PYR_{14}TFSI$, due to the lower viscosity[47,48] of the former.

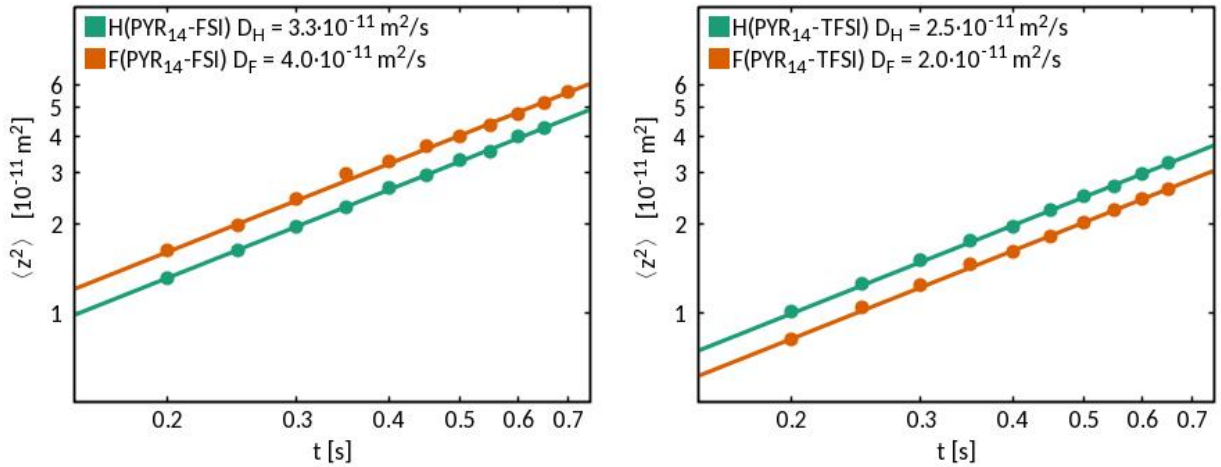

Figure 1. Log-log plot of the experimental MSDs $\langle z^2 \rangle$ for $PYR_{14}FSI$ (left panel) and $PYR_{14}TFSI$ (right panel), as a function of diffusion time *t*. Linear fits to the data are also shown, along with the diffusion coefficients.

To further assess the nature of the diffusive motion in both systems, we performed the *q-space* analysis, which leads to the displacement distribution profiles G_{NMR}. Note that the experimental data can only be collected over a finite range $0<q<q_{max}$, where the maximum value of q depends of investigated system (it is not necessary to record data for $q<0$, as $I(q,t)$ is necessarily an even function of q). The limited sampling in q-space usually leads to numerical fluctuations in the FT, which hamper the full reconstruction of the G_{NMR} profile. Zero filling or data extrapolation are commonly applied to overcome this issue and enhance the spatial resolution of the FT.[14] Here we adopt a different strategy, by fitting G_{NMR} to the FT of a truncated Gaussian with the same *q-space* interval. Thanks to the FT denoising properties, this procedure is expected to give more accurate results than fitting $I(q,t)$ via Eq. (2).

Figure 2 shows the results of the fitting of the experimental points for $PYR_{14}FSI$ and for diffusion times in the range 0.2-0.5 s. For both the cation and the anion, the agreement is excellent. The values of $\Delta(z_{0.5})$ decrease with decreasing diffusion times, as expected for a Gaussian diffusive behavior (see Eq. (6)). Similar results were obtained for $PYR_{14}TFSI$. This confirms the hypothesis of fully developed Gaussian diffusion of the ions on these long time-scales.

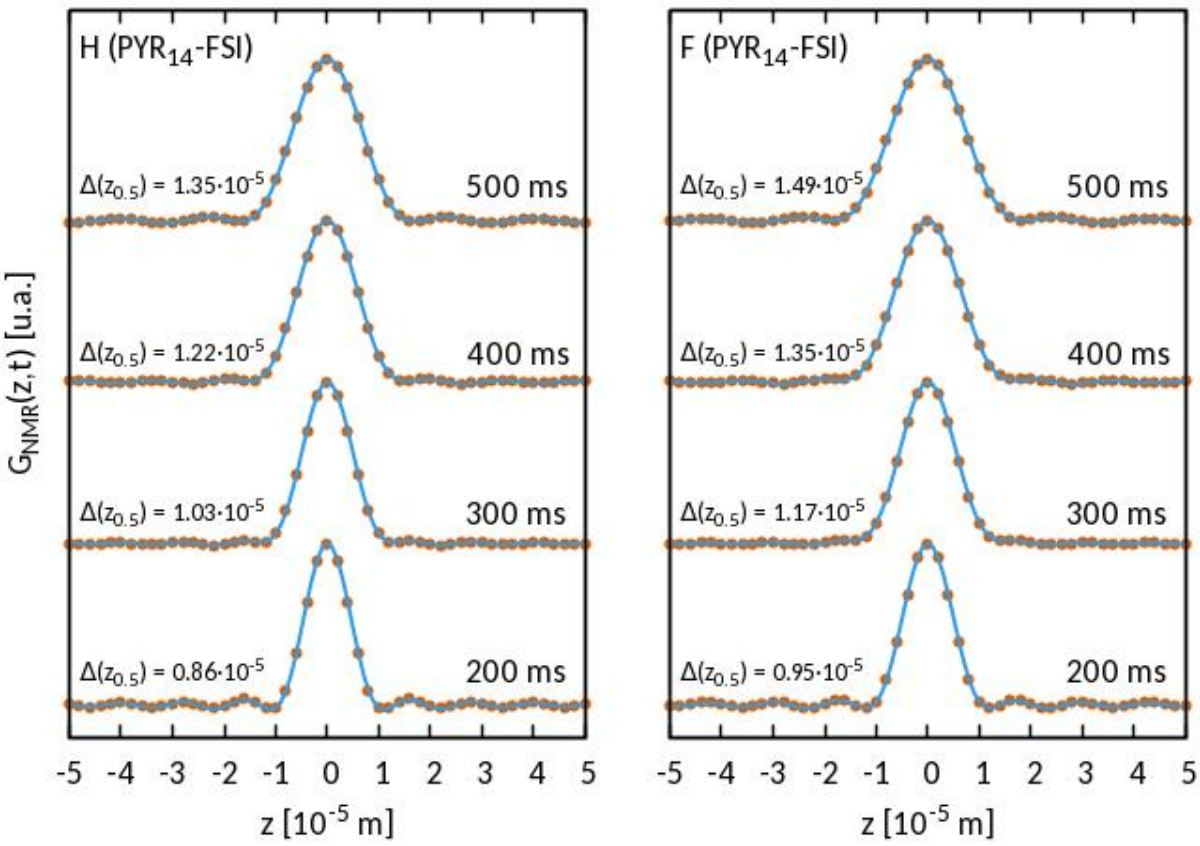

Figure 2. Displacement distribution profiles for H atoms (left) and F atoms (right) in $PYR_{14}FSI$. The numerical FTs of the original data (points) are compared with the fitted profiles at different diffusion times (lines). For comparison purposes, all functions have been rescaled to unity at z=0. Full widths at half-maximum are also reported.

To investigate the behavior of our systems on shorter timescales, which are not accessible to NMR, we performed classical MD simulations. All-atom force fields were developed for all species starting from the parameters by Canongia Lopez, Padua and coworkers.[49-52] The partial atomic charges were rescaled in order to obtain a good agreement between calculated and experimental RTILs densities (at 293 K)[4,5] and NMR diffusion coefficients at 305 K (see SI for

details), whilst maintaining the overall charge neutrality. The sum of atomic charges within the ions was ±0.6e for $PYR_{14}FSI$ and ±0.7e for $PYR_{14}TFSI$. This scaling is necessary mainly to correct for ion polarization effects, which are not included in our force field. Both RTIL models contained 125 cation/anion pairs. All simulations were performed at constant temperature and pressure, each with an overall duration of 0.5 μs.

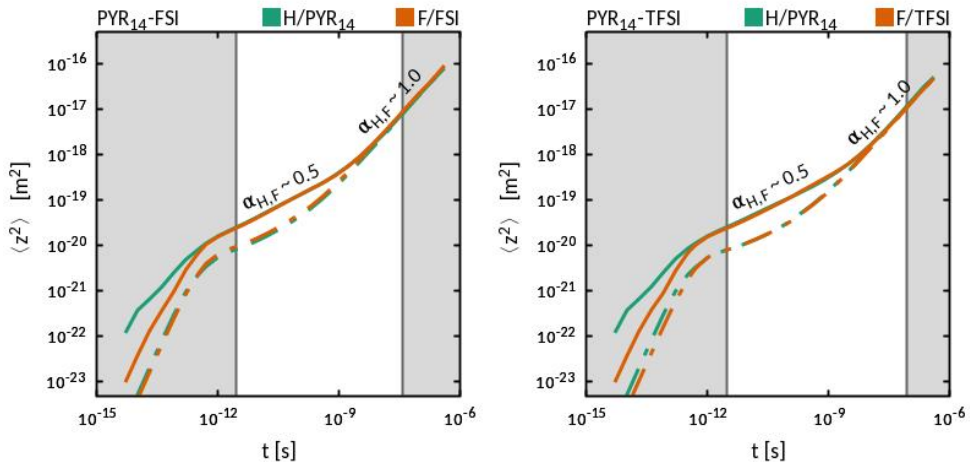

Figure 3. Log-log plot of $\langle z^2 \rangle$ for H and F atoms in $PYR_{14}FSI$ and $PYR_{14}TFSI$, derived from the MD simulations. Molecular center of mass profiles are shown as dashed lines. Shaded areas highlight the different diffusion regimes (see text). Approximate values of α for H and F within each region are also shown.

Figure 3 shows the mean-square displacements obtained from the MD simulations of both systems. In addition to the atom-based MSDs, which are closely analogous to those measured by NMR, we have plotted also the molecular center-of-mass (COM) displacements for the cations and anions. The changes of slope in the plots indicate the presence of three distinct diffusion regimes. The boundaries between them were set at the MSD inflection points, corresponding to the stationary points of $A(t) = \partial \log\langle z^2 \rangle / \partial \log(t)$. In both systems, the Fickian diffusive behavior (α=1) is observed for both H and F at times greater than about 10 ns. The MD

diffusion coefficients, calculated via Eq. (3) in the interval 10<t<400 ns and used for fine-tuning the force field parameters, are in excellent agreement with the experimental ones (see again Table 1).

Having validated the MD simulations by comparison with the long-time behavior encoded in the NMR data, we may analyze the ion dynamics at increasingly shorter times. Below 10 ns, corresponding to COM displacements of about 1.5 nm, the linear regime smoothly evolves into a subdiffusive regime, characterized by values of α close to 0.5 for H and F in both systems. The deviations from linearity affect in similar ways both RTILs, the subdiffusive regions spanning three orders of magnitude in time, from about 10 ns to about 3 ps. At very short times (t<3 ps) and displacements (of the order of 1 Å), the center of mass motion is free and characterized by a ballistic regime (α=2) analogous to that observed in other RTILs.[9,30] The corresponding atomic displacements are larger and associated with different values of α. Differences between atom-based and COM-based displacement are understandable at short times, since the former are sensitive to tumbling motions of the ions while the latter are not. For the same reason the differences between the short-time dynamics of the H and F atoms reflect different rotational, conformational and caging dynamics of the cations and anions. The minima of A(t), located at t_{min}=2.9 ps for all species, provide an estimate of the average collision time between nearest-neighbor molecules.

To further analyze the COM dynamics, we have calculated the corresponding Van Hove self-correlation functions:

$$G_{MD}(z,t)=\frac{1}{N}\left\langle \sum_{i=1}^{N}\delta\left(z+z_i(0)-z_i(t)\right)\right\rangle . \qquad (7)$$

Figure 4 compares the profiles of $G_{MD}(z,t)$ plotted as a function of the normalized displacement z/σ, σ being to the standard deviation of the displacements (square root of the MSD).[53] The

Gaussian distributions with the same variances are also plotted for comparison. For the largest diffusion time shown (t=12.8 ns), the deviation from the Gaussian behavior is generally small (except for TFSI), but progressively increase upon decreasing t. In analogy with more confined systems,[8,14,15] these deviations only affect the tails of the distributions, leaving the central portion unaffected.

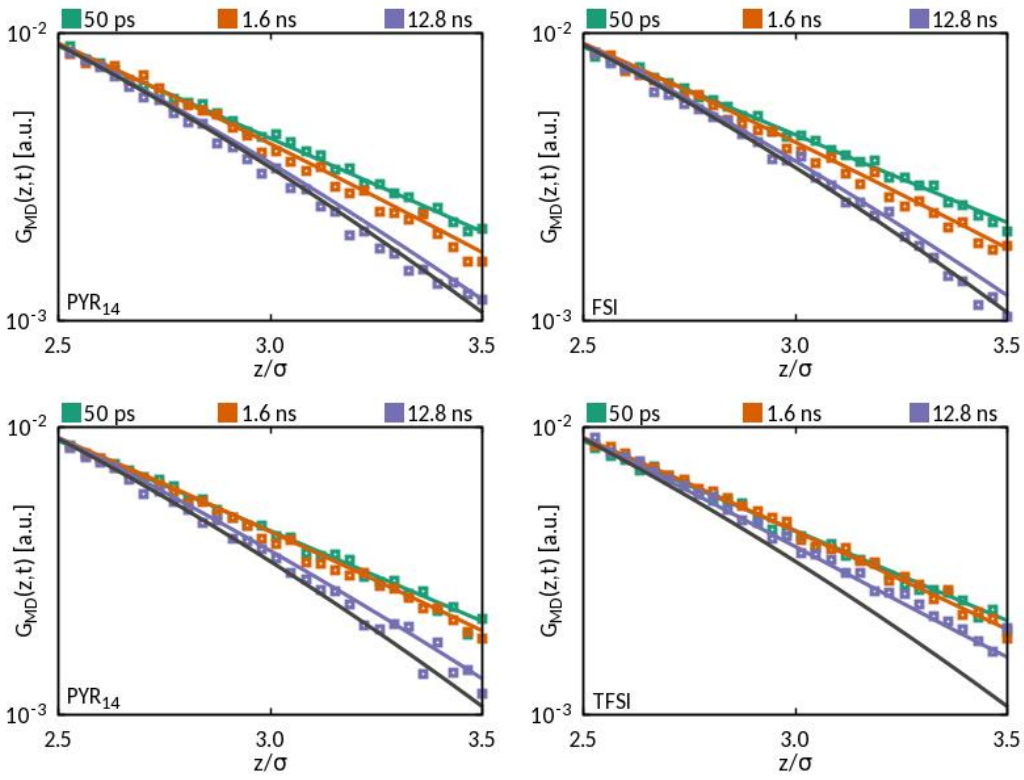

Figure 4: Normalized $G_{MD}(z,t)$, plotted logarithmically against the normalized displacement (z/σ) for PYR$_{14}$FSI (top) and PYR$_{14}$TFSI (bottom). Lines are fits to the data obtained with Lucy's deconvolution algorithm (see text). The black lines correspond to a Gaussian distribution with the same variance. For clarity, only the tails of the distribution with z/σ>2.5 are shown.

Decreasing the diffusion time, the tail distribution is found to decay linearly on the logarithmic plot, implying that the probability function changes according to $G_{MD}(z,t) \approx \exp(-|z|/\sigma)$. This behavior suggests the possibility of heterogeneity in long-range ($z/\sigma > 2.5$) diffusion processes, which could be described by admitting the existence of different ions' states with apparently different diffusion coefficients. In order to test this hypothesis, we have calculated the distribution of diffusivities, *P(D)*, using Lucy's deconvolution algorithm to fit the displacement distributions according to the following equation:[54]

$$G_{MD}(z,t) = \int P(D) \frac{e^{-z^2/4Dt}}{\sqrt{4\pi Dt}} dD \tag{8}$$

Eq. (8) describes $G_{MD}(z,t)$ as the superposition of Gaussian diffusion processes associated with different diffusion coefficients.[10] In this work, the integration was performed over a "basis set" of 400 Gaussian functions. In order to limit the statistical noise of poorly sampled regions, the integration interval was set to $-3.5 < z/\sigma < 3.5$. The result of the fitting are reported in Figure 4, whereas the corresponding diffusivities are given in Figure 5. For comparison purposes, we also report within Figure 5 the average diffusivities, given by:

$$D_{ave} = \int DP(D)dD \tag{9}$$

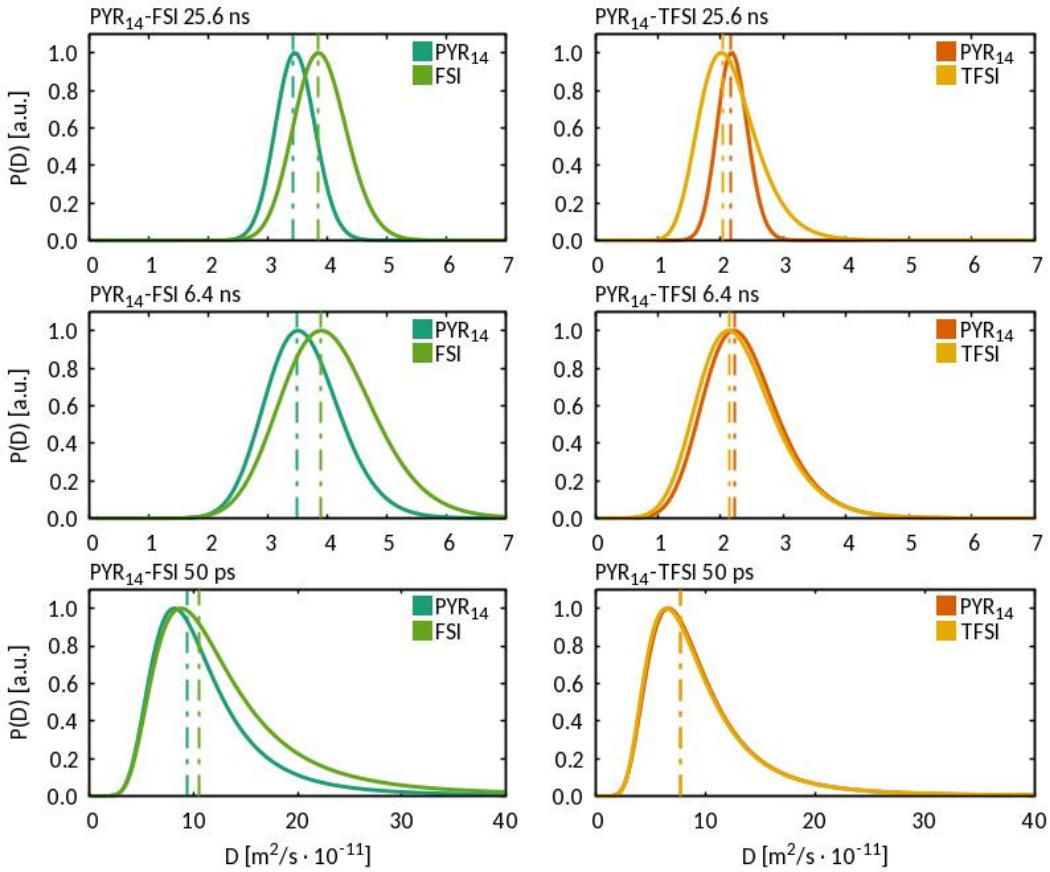

Figure 5. Diffusivity profiles of $PYR_{14}FSI$ and $PYR_{14}TFSI$ at different diffusion times. Dotted lines represent the average diffusion coefficients, D_{ave}. Note the different diffusivity ranges used to plot the data.

Before discussing these results, we note that, for a pure Gaussian motion, the use of Eq. (8) should provide an infinitely narrow delta function centered at D_{ave}. Clearly, this outcome cannot be observed, due the use of a finite number of Gaussians. Nonetheless, upon approaching the Gaussian behavior, we may also expect *P(D)* to converge to D_{ave}. For t = 25.6 ns, the diffusivity profiles are symmetrical and centered about the corresponding averages. The exception of TFSI is due to the slow converging behavior of its diffusion coefficient, as reported above. At 6.4 ns, the profiles look slightly asymmetrical for all species, although peak values are still centered on their averages. Interestingly, the cation and the anion in $PYR_{14}TFSI$ show

similar profiles, while in $PYR_{14}FSI$ the two profiles do not overlap. At 50 ps, in the subdiffusive domain, peak values no longer coincide with the averages. The profiles appear more skewed and span a wide range of diffusivities. This outcome can be associated with caging effects. The collisions with the neighbor ions increase the occurrence of small displacements, leading to the peaks at reduced *D*'s. Meanwhile, occasional cage rearrangements may promote large displacements. For t = 50 ps, we see that cation and anion diffusivities can be four times the peak value. Further analysis of the MD trajectories is reported in the SI.

Overall, the analysis of the experimental PGSE NMR data using two specific, but complementary approaches demonstrates that ion diffusion in $PYR_{14}TFSI$ and $PYR_{14}FSI$ is Gaussian over long observation timescales (ms). Conversely, molecular dynamics simulations indicate subdiffusive motion for short observation times (below 10 ns). This non-Gaussian dynamics is related to molecular caging effects. Work is in progress to extend this dual experimental-numerical approach to other systems, in particular ones with locally heterogeneous environments in which strong confinement effect have already been evidenced by experiments.[31]

ASSOCIATED CONTENT

Supporting Information. Experimental details for the acquisition and processing of the NMR data. Details on the Molecular Dynamics procedures. This material is available free of charge via the Internet at http://pubs.acs.org.

REFERENCES

(1) Angell, C. A.; Byrne, N.; Belieres, J.-P. Parallel Developments in Aprotic and Protic Ionic Liquids: Physical Chemistry and Applications. *Acc. Chem. Res*. **2007**, *40*, 1228–1236.

(2) Armand, M.; Endres, F.; MacFarlane, D.R.; Ohno, H.; Scrosati, B. Ionic-Liquid Materials for the Electrochemical Challenges of the Future. *Nat. Mater*. **2009**, *8*, 621–629.

(3) Simon, P.; Gogotsi, Y. Materials for Electrochemical Capacitors. *Nat. Mater*. **2008**, *7*, 845–854.

(4) Doroodian, A.; Dengler, J. E.; Genest, A.; Reosch, N.; Rieger, B. Methylguanidinium Borohydride: An Ionic-Liquid-Based Hydrogen-Storage Material. *Angew. Chem. Int. Ed.* **2010**, *49*, 1871–1873.

(5) Van Rantwijk, F.; Sheldon, R. A. Biocatalysis in Ionic Liquids. *Chem. Rev*. **2007**, *107*, 2757–2785.

(6) Stracke, M. P.; Ebeling, G.; Catalu~na, R.; Dupont, J. Hydrogen-Storage Materials Based on Imidazolium Ionic Liquids. *Energy Fuels* **2007**, *21*, 1695–1698.

(7) Castiglione, F.; Famulari, A.; Raos, G.; Meille, S. V.; Mele, A.; Appetecchi, G. B.; and Passerini, S. Pyrrolidinium-Based Ionic Liquids Doped with Lithium Salts: How Does Li+ Coordination Affect Its Diffusivity? *J. Phys. Chem B* **2014**, *118*, 47 13679-13688.

(8) Menjoge, A Dixon, J.; Brennecke, J. F.; Maginn, E. J.; and Vasenkov, S. Influence of Water on Diffusion in Imidazolium-Based Ionic Liquids: A Pulsed Field Gradient NMR study. *J. Phys. Chem. B* **2009**, *113*, 6353–6359.

(9) Del Popolo, M. G.; and Voth, A. G. On the Structure and Dynamics of Ionic Liquids, *J. Phys. Chem. B* **2004**, *108*, 1744-1752.

(10) Hu, Z.; Margulis, C. J. Room-Temperature Ionic Liquids: Slow Dynamics, Viscosity, and the Red Edge Effect. *Acc. Chem. Res*. **2007**, *40*, 1097-1105.

(11) Koddermann, T.; Ludwig, R.; and Paschek, D. On the Validity of Stokes-Einstein and Stokes-Einstein-Debye Relations in Ionic Liquids and Ionic-Liquid Mixtures. *Chem. Phys. Chem.,* **2008**, *9*, 1851-1858.

(12) Ishida, T.; and Shirota, H.; Dicationic versus Monocationic Ionic Liquids: Distinctive Ionic Dynamics and Dynamical Heterogeneity. *J. Phys. Chem. B* **2013**, *117*, 1136-1150.

(13) Willcox, J. A. L.; Kima, H.; and Kim, H. J.; A Molecular Dynamics Study of the Ionic Liquid, Choline Acetate. *Phys. Chem. Chem. Phys,* **2016**, *18*, 14850-14858.

(14) Hu, Z.; Margulis, C. J.; Heterogeneity in a Room-Temperature Ionic Liquid: Persistent Local Environments and the Red-Edge Eeffect. *Proc. Natl. Acad. Sci.* **2006**, *103*, 831-836.

(15) Berthier, L. Dynamic Heterogeneity in Amorphous Materials, *Physics* **2011**, 4, 42-49.

(16) Pastore, R.; Coniglio, A.; and Pica Ciamarra, M. From Cage-Jump Motion to Macroscopic Diffusion in Supercooled Liquids. *Soft Matter* **2014**, *10*, 5724-5728.

(17) Pastore, R.; Coniglio, A.; Pica Ciamarra, M. Dynamic Phase Coexistence in Glass-Forming Liquids. *Sci. Rep*. **2015**, 5, 11770-11780 .

(18) Larini L.; Ottochian, A; De Michele, C.; Leporini, D. Universal Scaling between Structural Relaxation and Vibrational Dynamics in Glass-Forming Liquids and Polymers. *Nat. Phys*. **2008**, *4*, 42-45.

(19) Weeks, E. R.; Crocker, J. C.; Levitt, A. C.; Schofield, A.; Weitz, D. A. Three-Dimensional Direct Imaging of Structural Relaxation Near the Colloidal Glass Transition. *Science* **2000**, *287*, 627-631.

(20) Gao, Y.; and Kilfoil, M. L. Direct Imaging of Dynamical Heterogeneities near the Colloid-Gel Transition. *Phys. Rev. Lett.* **2007**, 99, 078301-4.

(21) Kegel, W. K.; and van Blaaderen, A. Direct Observation of Dynamical Heterogeneities in Colloidal Hard-Sphere Suspensions. *Science* **2000**, *287*, 290-293.

(22) Wang, B.; Kuo, J.; Bae S. C.; and Granick, S. When Brownian Diffusion is not Gaussian. *Nature Mat*. **2012**, *11*, 481-485.

(23) Wang, B.; Anthony, S. M.; Bae, S. C.; and Granick, S. Anomalous yet Brownian, *Proc. Natl. Acad. Sci.* **2009**, *106*, 15160-15164.

(24) Hayes, R.; Warr, G.G.; and Atkin, R. Structure and Nanostructure in Ionic Liquids. *Chem. Rev.* **2015**, *115*, 6357-6426.

(25) Russina, O.; Lo Celso, F.; Plechkova, N. V.; and Triolo, A. Emerging Evidences of Mesoscopic-Scale Complexity in Neat Ionic Liquids and Their Mixtures. *J. Phys. Chem. Lett.* **2017**, *8*, 1197-1204.

(26) Koddermann, T.; Paschek, D.; and Ludwig, R. Molecular Dynamic Simulations of Ionic Liquids:A Reliable Description of Structure, Thermodynamics and Dynamics, *Chem. Phys. Chem.* **2007**, *8*, 2464-2470.

(27) Chen, S.; Zhang, S.; Liu, X.; Wang, J.; Wang, J.; Dong, K.; Sun, J.; Xu, B. Ionic Liquid Clusters: Structure, Formation Mechanism, and Effect on the Behavior of Ionic Liquids. *Phys. Chem. Chem. Phys.* **2014**, *16*, 5893-5906.

(28) Pereiro, A. B.; Pastoriza-Gallego, M. J.; Shimizu, K.; Marrucho, I. M.; Canongia Lopes, J. N.; Maneiro, M.; and Rebelo, L. P. N. On the Formation of a Third, Nanostructured Domain in Ionic Liquids, *J. Phys. Chem. B* **2013**, *117*, 10826-10833.

(29) Sha, M.; Liu, Y.; Dong, H.; Luo, F.; Jiang, F.; Tang, Z.; Zhud G.; and Wu, G. Origin of Heterogeneous Dynamics in Local Molecular Structures of Ionic Liquids, *Soft Matter* **2016**, *12*, 8942-8947.

(30) Sarangi, S. S.; Zhao, W.; Muller-Plathe, F.; and Balasubramanian, S. Correlation between Dynamic Heterogeneity and Local Structure in a Room-Temperature Ionic Liquid: A Molecular Dynamics Study of [bmim][PF_6], *Chem. Phys. Chem.* **2010**, *11*, 2001-2010.

(31) Ferdeghini, F.; Berrod, Q.; and Zanotti, J.-M.; Judeinstein, P.; Sakai, V. G.; Czakkel, O.; Fouquet, P.; and Constantin, D. Nanostructuration of Ionic Liquids: Impact on the Cation Mobility. A Multi-Scale Study, *Nanoscale* **2017**, *9*, 1901-1908.

(32) Aoun, B.; Gonzalez, M. A.; Ollivier, J.; Russina,M.; Izaola,Z.; Price, D. L.; and Saboungi, M.-L. Translational and Reorientational Dynamics of an Imidazolium-Based Ionic Liquid. *J. Phys. Chem. Lett.* **2010**, *1*, 2503-2507.

(33) Burankova, T.; Hempelmann, R.; Wildes, A.; and Embs, J. P. Collective Ion Diffusion and Localized Single Particle Dynamics in Pyridinium-Based Ionic Liquids. *J. Phys. Chem. B* **2014**, *118*, 14452-14460.

(34) Kim, G.-T.; Jeong, S.S.; Xue, M.-Z.; Balducci, A.; Winter, M.; Passerini, S.; Alessandrini, F.; Appetecchi, G. B. Development of Ionic Liquid-Based Lithium Battery Prototypes. *Journal of Power Sources* **2012**, *199*, 239-246.

(35) Kunze, M.; Jeong, S.; Paillard, E.; Winter, M.; and Passerini, S. Melting Behavior of Pyrrolidinium-Based Ionic Liquids and Their Binary Mixtures. *J. Phys. Chem. C* **2010**, *114*, 12364-12369.

(36) Castiglione, F.; Appetecchi, G. B.; Passerini, S.; Panzeri, W.; Indelicato, S.; Mele, A. Multiple Points of View of Heteronuclear NOE: Long Range *vs* Short Range Contacts in Pyrrolidinium Based Ionic Liquids in the Presence of Li Salts. *Journal of Molecular Liquids* **2015**, *210*, 215-222.

(37) Appetecchi, G.B.; Kim, G.T.; Montanino, M.; Alessandrini, F.; Passerini, S. Room Temperature Lithium Polymer Batteries Based on Ionic Liquids. *Journal of Power Sources* **2011**, *196*, 6703-6709.

(38) Nicotera, I.; Oliviero, C.; Henderson, W. A.; Appetecchi, G. B.; Passerini, S. NMR Investigation of Ionic Liquid-LiX Mixtures: Pyrrolidinium Cations and TFSI-Anions. *J. Phys. Chem. B* **2005**, *109*, 22814-22819.

(39) Castiglione, F.; Moreno, M.; Raos, G.; Famulari, A.; Mele, A.; Appetecchi, G. B.; and Passerini, S. Structural Organization and Transport Properties of Novel Pyrrolidinium-Based

Ionic Liquids with Perfluoroalkyl Sulfonylimide Anions. *J. Phys. Chem. B* **2009**, *113*, 10750-10759.

(40) Mele, A.; Romano, G.; Giannone, M.; Ragg, E.; Fronza, G.; Raos, G.; Marcon, V. The Local Structure of Ionic Liquids: Cation-Cation NOE Interactions and Internuclear Distances in Neat [BMIM][BF_4] and [BDMIM][BF4]. *Angew. Chem., Int. Ed.* **2006**, *45*, 1123-1126.

(41) Marincola, F. C.; Piras, C.; Russina, O.; Gontrani, L.; Saba, G.; Lai, A. NMR Investigation of Imidazolium-Based Ionic Liquids and Their Aqueous Mixtures. *Chem. Phys. Chem.* **2012**, *13*, 1339-1346.

(42) Headley, A. D.; Jackson, N. M. The Effect of the Anion on the Chemical Shifts of the Aromatic Hydrogen Atoms of Liquid 1-Butyl-3-Methylimidazolium Salts. *J. Phys. Org. Chem.* **2002**, *15*, 52-55.

(43) Borodin, O.; Gorecki, W.; Smith, G. D.; and Armand, M. Molecular Dynamics Simulation and Pulsed-Field Gradient NMR Studies of Bis(fluorosulfonyl)imide (FSI) and Bis[(trifluoromethyl)sulfonyl]imide (TFSI)-Based Ionic Liquids. *J. Phys. Chem. B* **2010**, *114*, 6786-6798.

(44) Callaghan, P. T.; Codd, S. L.; Seymour, J. D. Spatial Coherence Phenomena Arising from Translational Spin Motion in Gradient Spin Echo Experiments. *Concepts Magn. Reson*. **1999**, *11*, 181-202.

(45) Cohen, Y.; Assaf, Y. High b-Value q-Space Analyzed Diffusion-Weighted MRS and MRI in Neuronal Tissues – a Technical Review. *NMR Biomed*. **2002**, *15*, 516-542.

(46) Cory, D. G.; Garroway, A. N. Measurement of Translational Displacement Probabilities by NMR An Indicator of Compartmentation. *Magn. Reson. Med*. **1990**, *14*, 435-444.

(47) Zhou, Q.; Henderson, W.A.; Appetecchi, G.B.; Montanino M.; and Passerini S. Physical and electrochemical properties of N-Alkyl-N-methylpyrrolidinium bis(fluorosulfonyl)imide ionic liquids: $PYR_{13}FSI$ and $PYR_{14}FSI$. *J. Phys. Chem. B,* **2008**, *112*, *13577-13580*.

(48) Appetecchi, G.B.; Montanino, M.; Carewska, M.; Moreno, M.; Alessandrini, F.;. Passerini, S. Chemical-physical properties of bis(perfluoroalkylsulfonyl)imide anion-based ionic liquids. *Electrochimica Acta*, **2011**, *56*, *1300-1307*.

(49) Canongia Lopes, J. N. Modeling Ionic Liquids Using a Systematic All-Atom Force Field. *J. Phys. Chem. B* **2004**, *108*, 2038-2047.

(50) Canongia Lopes J. N. and Padua, A. A. H. Molecular Force Field for Ionic Liquids III: Imidazolium, Pyridinium, and Phosphonium Cations; Chloride, Bromide, and Dicyanamide Anions. *J. Phys. Chem. B* **2006**, *110*, 19586-19592.

(51) Shimizu, K.; Almantariotis, D.; Costa Gomes, M. F.; Padua, A. A. H.; and Canongia Lopes, J. N. Molecular Force Field for Ionic Liquids V: Hydroxyethylimidazolium, Dimethoxy-2-Methylimidazolium, and Fluoroalkylimidazolium Cations and Bis(Fluorosulfonyl)Amide, Perfluoroalkanesulfonylamide, and Fluoroalkylfluorophosphate Anions. *J. Phys. Chem. B* **2010**, *114*, 3592-3600.

(52) Van Hove, L. Correlations in Space and Time and Born Approximation Scattering in Systems of Interacting Particles. *Phys. Rev*. **1954**, *95*, 249-262.

(53) Xue, C.; Zheng, X.; Chen, K.; Tian, Y.; and Hu, G. Probing Non-Gaussianity in Confined Diffusion of Nanoparticles, *J. Phys. Chem. Lett*. **2016**, *7*, 514-519.

(54) Lucy, L. B. An Iterative Technique for the Rectification of Observed Distributions. *Astron. J.* **1974**, *79*, 745-754.

(55) Bedrov, D.; Borodin, O.; Li, Z.; and Smith, G. D. Influence of Polarization on Structural, Thermodynamic, and Dynamic Properties of Ionic Liquids Obtained from Molecular Dynamics Simulations. *J. Phys. Chem. B* **2010**, *114*, 4984-4997